



Cite this: *Chem. Sci.*, 2020, **11**, 7015

All publication charges for this article have been paid for by the Royal Society of Chemistry

Received 5th May 2020
Accepted 16th June 2020

DOI: 10.1039/d0sc02533j
rsc.li/chemical-science

Introduction

One of the key challenges in the selective discrimination of polyanionic species is the lack of chemical or structural differences between homologous series. For example, the linear aliphatic dicarboxylates (malonate–azelate) have similar chemical properties in terms of pK_a and hydration enthalpies^{1,2} and differ only in terms of the length of the flexible aliphatic linker. Furthermore, polyanionic species exist preferentially in an aqueous environment, which adds further complications in the design of chemical entities for the selective discrimination of these species in their native environment. Because of their biological^{3–5} and industrial^{1,6,7} importance, the development of sensors which can selectively bind and detect polyanionic species is a significant challenge and has commanded special attention from the chemical community.

In nature, succinate dehydrogenase selectively binds succinate *via* 5-hydrogen bonds to each carboxylate unit, with additional stabilisation of the anion achieved by exclusion of water molecules from the binding site.^{8,9} Malonate is a known competitive inhibitor of this enzyme,¹⁰ demonstrating that even for the naturally evolved systems in biology, selective discrimination of dicarboxylates is troublesome. Nonetheless, there are many excellent examples in the literature of receptors that

utilise hydrogen,^{11–14} halogen¹⁵ and chalcogen bonds,¹⁶ ion-pairing interactions^{17,18} and metal–ligand interactions^{19,20} to discriminate di-(and multi)topic carboxylate species in competitive (and non-competitive) solvents with both macrocycles^{21–23} and cages²⁴ used to achieve some levels of dicarboxylate discrimination. More recently, arrays have been utilised to selectively detect ditopic anionic species,^{25–27} although these often require complex calibration.

One potential strategy for achieving selective ditopic anion binding involves investigating and optimising the role of chelate (or intramolecular) cooperativity. Chelate cooperativity describes the likelihood of the formation of discrete complexes in preference to higher order oligomers (Fig. 1).^{28–30} In the case of a ditopic host binding to a ditopic guest, chelate cooperativity refers to the formation of the fully bonded 1 : 1 complex, where the initial binding event (K_{ini}) at one ‘end’ of the complex brings the binding sites at the other ‘end’ into close proximity, thereby making the subsequent intramolecular binding event (K_{intra}) to give the 1 : 1 complex more likely to occur than oligomerisation processes (K_{inter}). If both binding sites in the ditopic receptor are identical, the three microscopic binding constants K_{ini} , K_{intra} and K_{inter} are deconvoluted into the monotopic reference binding constant (K_{ref}) and appropriate statistical coefficients to account for the degeneracy of the systems, while K_{intra} is defined by eqn (1) where σ' is the statistical coefficient and EM is the effective molarity; a correction factor to account for the intramolecular nature of the second binding step.

$$K_{\text{intra}} = \sigma' K_{\text{ref}} \times \text{EM} \quad (1)$$

School of Chemistry, The University of Sydney, NSW 2006, Australia. E-mail: Kate.Jolliffe@sydney.edu.au

† Electronic supplementary information (ESI) available: Providing details of the compound synthesis and characterization, UV-vis binding studies and fitted titration data, DMC analysis and derivatization, fluorescence screening studies, NMR titration data and crystallography methods (PDF). Crystallographic data for **dt2·Mal**, **dt2·Adi** and **dt2·Aze** (cif). CCDC 1954830–1954832. For ESI and crystallographic data in CIF or other electronic format see DOI: [10.1039/d0sc02533j](https://doi.org/10.1039/d0sc02533j)



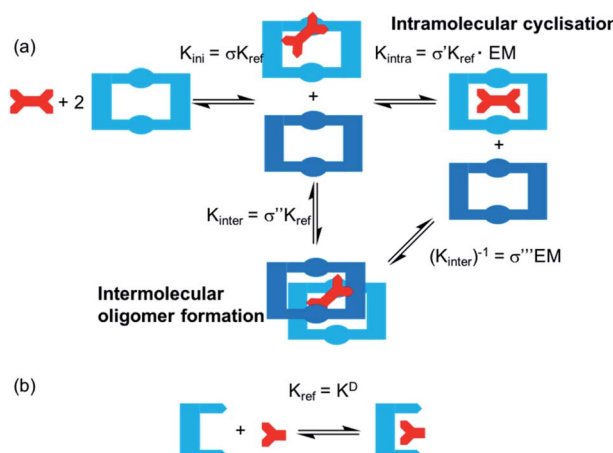


Fig. 1 (a) Schematic showing the stepwise binding of a ditopic guest to a ditopic macrocyclic receptor in presence of excess macrocycle. Rate constants shown define the microscopic binding constant for the initial binding step (K_{ini}) and the intramolecular cyclisation step (K_{intra}) or intermolecular oligomer formation (K_{inter}). (b) Binding of a monotopic reference guest to a monotopic host and definition of K_{ref} for this study.

complex), whereas K_{intra} values $\ll 1$ indicate negative cooperativity (*i.e.* favourable oligomer formation). While EM and K_{intra} cannot be measured directly, they can be determined using double mutant cycle (DMC) analyses, as described previously by Hunter,^{31–34} Schalley^{35–37} and others.^{38,39}

In recent years, several in-depth studies have revealed intriguing insights about the chelate cooperativity effect uncovering some of the range and limitations for which it may be utilised to design efficient supramolecular systems. Hunter and co-workers have shown that chelate cooperativity is enhanced in polar solvents over non-polar solvents due to sterically unfavourable interactions with competitive solvents which are relieved upon intramolecular ‘cyclisation’.³³ In addition, studies have focused on the effect of pre-organisation and rigidity of both hosts and guests.^{32,34–36,38,40} While highly pre-organised host/guest systems can yield very high EMs,⁴¹ often rigid host/guest systems with slight geometric mismatches suffer from much lower cooperative effects, as opposed to more flexible systems where the cooperative effect can remain strong over varied guest sizes due to the host undergoing a conformational change to adapt to guest size. This has led to the conclusion that often the synthetic effort required to produce highly pre-organised systems is not rewarded with strong cooperative effects, and more flexible systems may be useful in designing supramolecular motifs to achieve strong binding.

The majority of fundamental studies investigating chelate cooperativity to date have been conducted in relatively non-polar organic solvents, excluding potential competitive binding interactions arising from the solvent. Furthermore, most studies use charge or ion-pairing,^{17,42} in addition to hydrogen bonding to investigate the chelate effect. While these have provided valuable insights into the chelate effect, the application of the chelate effect in receptors designed for competitive solvent systems has been under explored. The aims

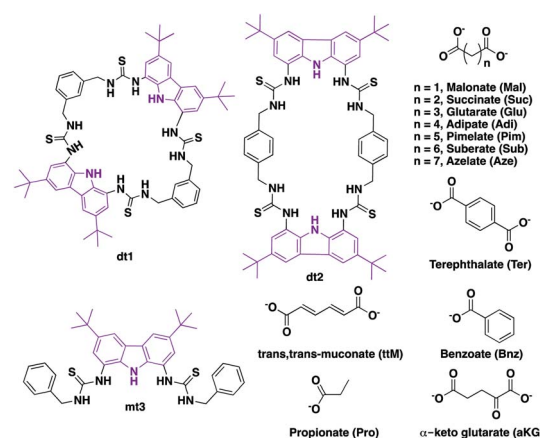
of the study described herein were two-fold: firstly, to investigate chelate cooperativity in neutral receptors that rely solely on hydrogen bonding interactions with anionic guests and secondly, to investigate the chelate cooperativity contributions in a highly competitive aqueous containing solvent medium. We envisaged that full analysis of the chelate cooperativity for binding of ditopic anions in competitive solvent systems would provide valuable insight into how to maximise the chelate effect, thereby greatly enhancing the development of selective and specific receptors/sensors for ditopic anions with real-world applications.

Results and discussion

Strategy

We chose to investigate dicarboxylate guests because the inherent difficulties in designing receptors capable of discriminating between these species makes these challenging targets for selective recognition. In order to accommodate both linear and rigid dicarboxylate guests, we designed our receptors to be semi-flexible, maintaining a certain degree of adaptability to better encapsulate their guest. We employed the 1,8-diamino carbazole scaffold, which has previously exhibited strong binding to oxoanions and should allow analysis of the binding event by UV-vis and fluorescence spectroscopy,^{43–45} in the design of two ditopic tetraethiourea macrocyclic species **dt1** (**ditopic 1**) and **dt2** (**ditopic 2**) (Scheme 1). The bis-carbazole units are linked by either 1,3-xylyl (**dt1**) or 1,4-xylyl (**dt2**) groups to vary macrocycle pore shape and also to provide semi-flexibility wherein the macrocycle can flex about the 4 methylene units.⁴⁶ As the reference compound for both macrocycles, we synthesised the open analogue **mt3** (**monotopic 3**). All receptors were synthesised in moderate yields (see ESI† for details).

As EM and K_{intra} cannot be measured experimentally, we employed the well-defined double mutant cycle (DMC) analysis to determine the individual components of each binding process (Fig. 2).³⁰ This approach has been described in detail previously for similar ditopic host/ditopic guest binding^{35,47} and



Scheme 1 Carbazole tetraethiourea macrocycles **dt1** (**ditopic 1**) and **dt2** (**ditopic 2**) and open bisthiourea carbazole **mt3** (**monotopic 3**) along with mono and dicarboxylate anions used in this study.

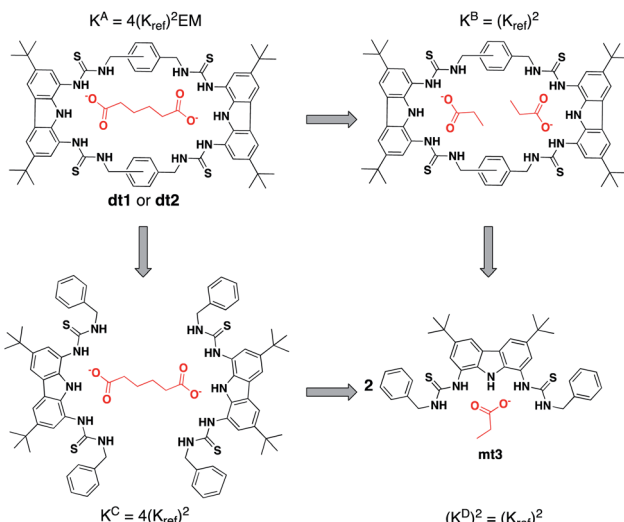


Fig. 2 Double mutant cycle for **dt1** or **dt2** with **Adi** as a representative guest. Equations show how each macroscopic binding constant is related to the binding of the reference host/guest system (K_{ref}).

full details of the DMC analysis conducted in this study including derivation of the equations to calculate EM and K_{intra} are provided in the ESI.[†]

For this study, two cuts or chemical mutations were applied to the macrocycle-anion complex, first to the macrocycle to create receptor **mt3**, and secondly to the ditopic anion, in which we used the monotopic **Pro** or **Bnz** (as the cut for **Ter**) for all analysis in this study.

DMC analysis allows all individual components of the binding event to be measured experimentally and expressed in terms of EM, the monovalent reference K_{ref} and statistical factors. By combining each mutation into an equilibrium (Fig. 3), the overall binding constant for the system can be calculated and subsequently EM (eqn (2)) and the apparent microscopic binding constant K_{intra} are derived (eqn (3)).

$$K = \frac{K^A (K^D)^2}{K^B K^C} = \text{EM} \quad (2)$$

$$K_{\text{intra}} = 1/2 K_{\text{ref}} \times \text{EM} \quad (3)$$

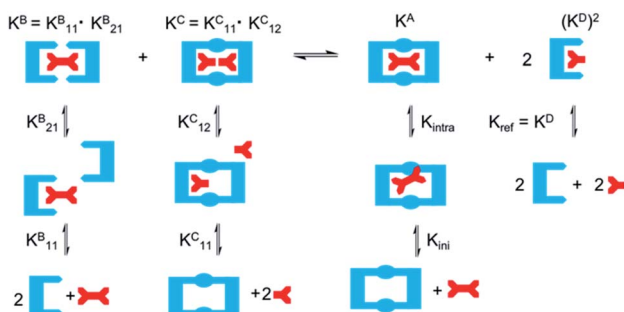


Fig. 3 Application of DMC analysis to calculate the overall binding constants for the binding of a ditopic host to a ditopic guest in this study.

Binding of ditopic hosts to guests

To initially investigate the spectroscopic responses of **dt1** and **dt2** to anions, fluorescence screening was carried out wherein 10 equivalents of various tetrabutylammonium anion salts (Cl^- , Br^- , I^- , PF_6^- , SO_4^{2-} , HCO_3^- , Bnz^- , OAc^- , Mal^{2-} , Suc^{2-} , Glu^{2-} , Adi^{2-} , Pim^{2-} , Sub^{2-} , Aze^{2-} , Ter^{2-} , ttM^{2-} and aKG^{2-}) were added to a 25 μM solution of **dt1** or **dt2** in aqueous DMSO solution ($\text{H}_2\text{O} : \text{DMSO} 1 : 9$ v/v) (ESI Fig. S63–S66[†]). Following excitation at 300 nm, fluorescence spectra were obtained. Generally, significant quenching was observed with ditopic anions and SO_4^{2-} , attributed to inhibition of the PET effect, whereas no or little quenching was observed with other anions, including monocarboxylates Bnz^- , OAc^- and HCO_3^- indicating that these ditopic receptors have a selective response for ditopic guests over monotopic guests.

The binding affinities of **dt1** and **dt2** towards TBA (tetrabutylammonium) salts of linear unsaturated dicarboxylates **Mal**–**Aze**, the rigid **Ter**, the benzene exposure biomarker **ttM** and Kreb's cycle intermediate **aKG** were measured by UV-vis titration in aqueous DMSO solution ($\text{H}_2\text{O} : \text{DMSO} 1 : 9$ v/v). Titration data was fitted to a 1 : 1 binding model using a global fitting analysis on the *Bindfit* web app⁴⁸ and are shown in Fig. 4 and Table 1 [fitted titration curves are provided in the ESI (Fig. S21–S41[†])]. In all cases, data fitted better to a 1 : 1 binding model over other models tested (1 : 2, 2 : 1 etc.) suggesting this was the likely binding mechanism to ditopic anions (*vide infra*). Throughout this study all titration data was fitted to all possible binding models, with the best model selected by evaluation of quality of the fit using residual analysis.

Interestingly, for the saturated linear dicarboxylate species (**Mal**–**Aze**), only minor discrepancies in binding affinity were observed between the two differently shaped receptors **dt1** and **dt2**. Both macrocycles exhibit the highest affinity for **Adi**, with strong 1 : 1 binding in the competitive aqueous solvent mixture used. In addition, both compounds display a similar selectivity pattern across the linear dicarboxylate series (**Mal**–**Aze**). This surprising result is attributed to the flexibility of *m*-xylyl linked (**dt1**) or *p*-xylyl linked (**dt2**) receptors. Although the two

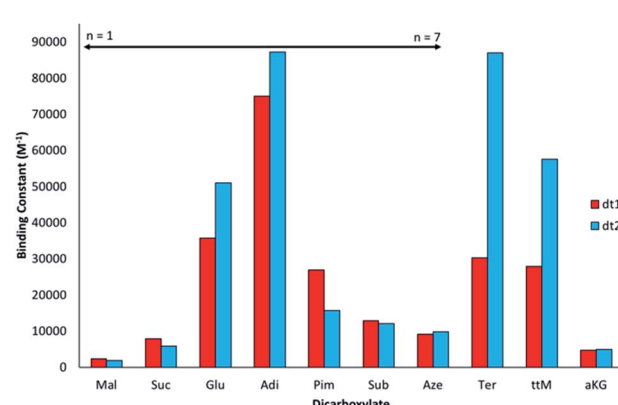


Fig. 4 Graphical representation of macroscopic binding constants for macrocycles **dt1** and **dt2** with dicarboxylates in aqueous DMSO solution ($\text{H}_2\text{O} : \text{DMSO} 1 : 9$ v/v) determined by UV-vis titration at 298 K and fitted to a 1 : 1 binding model.



Table 1 Double mutant cycle analysis for macrocycles **dt1** and **dt2**. UV-vis titrations were performed in aqueous DMSO solution ($\text{H}_2\text{O} : \text{DMSO}$ 1 : 9 v/v) and data fitted to an appropriate model by conducting a global fitting analysis using Bindfit.⁴⁸ Anions were added as tetrabutylammonium (TBA) or (TBA)₂ salts

mt3			dt1			dt2		
Anion	$n =$	$K_{11}^a (\text{M}^{-1})$	$K_{\text{A}}^b (\text{M}^{-1})$	EM ^c (mM)	$K_{\text{intra}}^d (\text{M}^{-1})$	$K_{\text{A}}^b (\text{M}^{-1})$	EM ^c (mM)	$K_{\text{intra}}^d (\text{M}^{-1})$
Pro	—	600 ^b	3300 (830) ^e	—	—	2300 (1200) ^f	—	—
Bnz	—	1800 ^b	30 000 (480) ^f	—	—	19 000 (200) ^f	—	—
Mal	1	1600	2300	0.5	0.15	1900	0.4	0.12
Suc	2	550	7900	14	4.2	5800	10	2.9
Glu	3	1000	36 000	21	6.2	51 000	28	8.5
Adi	4	660	75 000	91	27.4	87 000	102	30.7
Pim	5	1100	27 000	12	3.7	16 000	7	2.1
Sub	6	2100	13 000	1.6	0.5	12 000	1.5	0.5
Aze	7	1400	9000	2.5	0.8	10 000	2.6	0.8
ttM	—	680 ^g	28 000	32	9.7	58 000	64	19.3
Ter	—	1200	30 000	19	17.4	87 000	210	191.4
aKG	—	n/d ^h	4600	n/d ^h	n/d ^h	5000	n/d ^h	n/d ^h

^a All errors $\pm 15\%$. K_{11} as determined by UV-vis titration with data fitted to a 2 : 1 statistical binding model. ^b Macroscopic association constant as determined by fitting data to a 1 : 1 binding model. ^c Effective molarity determined by double mutant cycle (DMC) analysis. See ESI Section 5 for more information. ^d K_{intra} as determined by eqn (3) and by DMC analysis. ^e Data fitted to a 1 : 2 statistical model, K_{12} is shown in parenthesis. ^f Data fitted to a full 1 : 2 model, K_{12} is shown in parenthesis. ^g Data fitted using single peak analysis at 360 nm. ^h Not determined.

macrocycles have differing pore shapes, with saturated dicarboxylate guests both the host and guest are adaptable, and similar binding constants are observed for the two receptors. **Adi** ($n = 4$), with the highest binding affinity appears to be the optimal guest from the saturated dicarboxylate series for both macrocycles. With anions larger than **Adi**, the binding strength drops off sharply, presumably as the anion becomes too big to fit fully inside the macrocyclic pore. Notably, **dt2** exhibits selectivity of almost one order of magnitude between anions two carbon chains smaller (**Suc**, $n = 2$) or larger (**Sub**, $n = 6$) than **Adi**.

In contrast to the behaviour observed with flexible guests, when evaluating the binding to the rigid dicarboxylates the two macrocycles differ markedly in their binding affinities. The *p*-xylyl linked macrocycle **dt2** binds **Ter** with a high affinity ($K_{\text{a}} = 87\ 000\ \text{M}^{-1}$) in contrast to **dt1**, for which binding is three times weaker ($K_{\text{a}} = 30\ 000\ \text{M}^{-1}$). This result suggests **Ter**, which is conformationally rigid, is a good geometric match to **dt2** and a slight mismatch with the more ‘squashed’ pore of **dt1**. Likewise, a similar effect was observed with **ttM**, which is also conformationally restricted due to the restricted rotation around the double bonds. In this instance, **dt2** ($K_{\text{a}} = 58\ 000\ \text{M}^{-1}$) binds **ttM** twice as strongly as **dt1** ($K_{\text{a}} = 28\ 000\ \text{M}^{-1}$). It was hypothesised that the extra carbonyl group in **AKG** might provide an extra binding site for the hydrogen-bonding groups, however, for both macrocycles, the binding was considerably lower than binding to **Glu**, which has the same distance between the carboxylate groups. This may be due to unfavourable steric effects in accommodating the anion within the macrocyclic binding site.

To confirm the binding mechanism, we performed ¹H NMR titration experiments in DMSO-d₆/0.5% H₂O. For both macrocycles, with **Adi** we observed slow exchange up to 1 equivalent of

guest and subsequently no further changes in ¹H NMR spectra (Fig. 5 for **dt2** and ESI Fig. S70† for **dt1**). Further, sharpening of the methylene protons (H₆) which initially appear broad was observed, indicating a conformational change is occurring upon binding to **Adi** which brings all 8 methylene protons to a chemically equivalent environment in the 1 : 1 complex. Interestingly, a similar effect was observed when investigating **dt2** with the largest anion in the series, **Aze** (ESI Fig. S69†). Conversely however, with **dt2** and the smallest anion, **Mal**, intermediate exchange was observed, suggesting a much weaker binding event, confirming the UV-vis titration results (ESI Fig. S67†). For **dt1** with **Mal**, intermediate exchange was also observed up to addition of 1 equivalent of anion, with

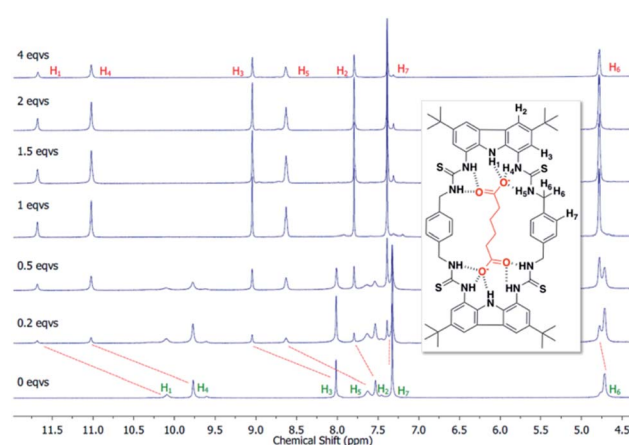


Fig. 5 Stack plot showing the aromatic region from the ¹H NMR titration of **dt2** with **Adi** in DMSO/0.5% H₂O at 298 K along with proton assignment. Slow exchange is displayed, indicative of strong 1 : 1 binding.



further peak splitting at higher guest concentrations, suggesting that higher order complexes (oligomers) may also be formed in this case (ESI Fig. S71†). Attempts to fit the UV-vis titration data to higher order binding models (2 : 1 and 1 : 2 models) for the titrations with **Mal** produced poor fits which were rejected. It is possible that the more competitive solvent used in UV-vis titration studies along with the much lower concentrations inhibits the formation of higher order complexes which could form in the NMR studies.

Double mutant cycle analysis

Next, we performed full DMC analysis for receptors **dt1** and **dt2** by conducting UV-vis titrations in aqueous DMSO solution ($\text{H}_2\text{O} : \text{DMSO} 1 : 9$ v/v) of **mt3** and the full range of dicarboxylates, as well as of **dt1** and **dt2** with the monotopic guests, propionate and benzoate, as summarised in Table 1. In the DMC analysis, TBA propionate (**Pro**) was used as the monotopic guest mimic for all dicarboxylates with the exception of **Ter**, in which TBA benzoate (**Bnz**) was used. The chelate cooperativity effect becomes clear when the DMC analysis is assessed. Whereas the monotopic receptor **mt3** binds the monotopic anion **Pro** with a low to moderate association constant in the order 10^3 M^{-1} , the ditopic receptors can reach association constants approaching 10^5 M^{-1} with ditopic guests, more precisely, **dt2** binds **Adi** 175 times stronger than **mt3** binds **Pro**.

Analysis of the effective molarities (EM) and K_{intra} for this system allows several conclusions to be drawn. Interestingly, as with the initial binding constant analysis of **dt1** and **dt2** with ditopic anions, there are few discrepancies in the cooperativity trend between the two macrocycles. Fig. 6 shows a graphical representation of $\log(K_{\text{intra}})$ whereby if $\log(K_{\text{intra}}) < 0$, negative cooperativity is observed, and likewise if $\log(K_{\text{intra}}) > 0$, positive cooperativity is observed.

For both macrocycles, with **Mal**, low K_{intra} values are obtained. This is because **Mal** is too short to span the width of both macrocycles and efficiently form a 1 : 1 complex, therefore, oligomer formation is favourable. Likewise, with the largest two dicarboxylates **Sub** and **Aze**, K_{intra} values $< 1 \text{ M}^{-1}$ are observed

indicating the formation of oligomers is favoured over the 1 : 1 complex. In this case, both anions are much too large for both hosts and therefore would have to bend significantly to bind both sides of the macrocycle, which would result in a significant entropic penalty resulting in favourable oligomer formation.

For anions with intermediate binding strengths towards the macrocycle (**Suc**, **Glu** and **Pim**), K_{intra} values of less than 10 are observed, together with moderate EM values. This suggests modest positive cooperativity with equilibria shifted towards cyclised 1 : 1 complex formation, despite an imperfect size match. With the strongest binding linear dicarboxylate **Adi**, high K_{intra} values are observed, indicating strong positive cooperativity towards both macrocycles, along with EMs of $\sim 100 \text{ mM}$. Interestingly, the favourable chelate cooperativity drops away rapidly with increasing anion length above the optimal with K_{intra} **Pim** ~ 7 (**dt1**) and 15 (**dt2**) times lower than K_{intra} **Adi**. A possible reason for this rapid drop off in cooperativity above the optimal anion size could be due to favourable spacer effects arising from additional stabilisation gained if the alkyl spacer on the guest can be fully encapsulated by the host. If a longer guest has to bend or flex to induce a fit inside the macrocycle pore, some of the alkyl spacer will be exposed to the bulk solvent, which may destabilise the ditopically bound species resulting in less favourable cooperative effect.

Differences in cooperativity between the two differently shaped macrocycles are observed with rigid anions. With **ttM**, **dt2** exhibits strong positive cooperativity, which is also reflected by a high binding constant. Conversely, for **dt1** only moderate cooperativity is observed. For binding to **Ter**, in which **Bnz** was taken as the reference guest, **dt2** shows the highest positive chelate cooperativity for the series with an EM value of 210 mM and K_{intra} approaching 200 M^{-1} . This high positive cooperativity is attributed to a combination of excellent geometric match between **dt2** and **Ter**, together with favourable $\pi-\pi$ interactions between the central aromatic rings on the macrocycle and the aromatic guest. **dt1** with **Ter** also exhibits reasonably strong positive cooperativity, which again could be a result of stabilisation through favourable $\pi-\pi$ interactions. Further evidence for favourable aromatic stabilisation comes from closer examination of the DMC data. Whilst the monotopic **mt3** binds **Bnz** with moderate affinity ($K_a = 1800 \text{ M}^{-1}$), both ditopic hosts exhibit a K_{11} binding constant an order of magnitude higher ($K_{11} = 30\,000 \text{ M}^{-1}$ for **dt1** and $19\,000 \text{ M}^{-1}$ for **dt2**), suggesting favourable stabilisation of this monotopic guest within the macrocycle. Nonetheless, **dt2** exhibits an order of magnitude higher K_{intra} than **dt1** towards **Ter** which can be attributed to a better geometric match of the receptor to the guest length.

Crystal structure analysis

Single crystals of **dt2** with three different dicarboxylates of various lengths suitable for X-ray crystal structure analysis were obtained (Fig. 7). The crystal structures confirmed the binding mode of the macrocycles, in which each carboxylate unit is bound by 5 hydrogen bonds stemming from the two thiourea groups and the central carbazole NH of each binding site.

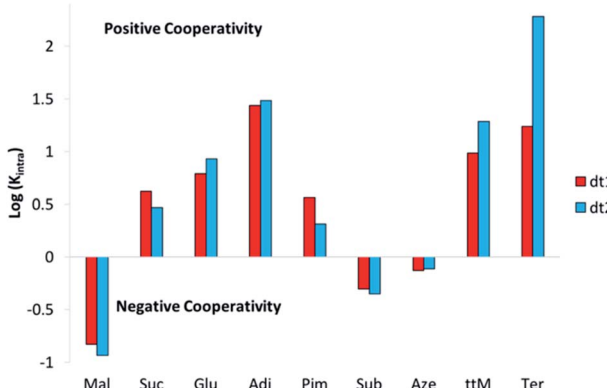


Fig. 6 Graphical representation of $\log(K_{\text{intra}})$ for **dt1** and **dt2** where positive values indicate positive cooperativity (favourable cyclisation) and negative values indicate negative cooperativity (favourable oligomerisation).



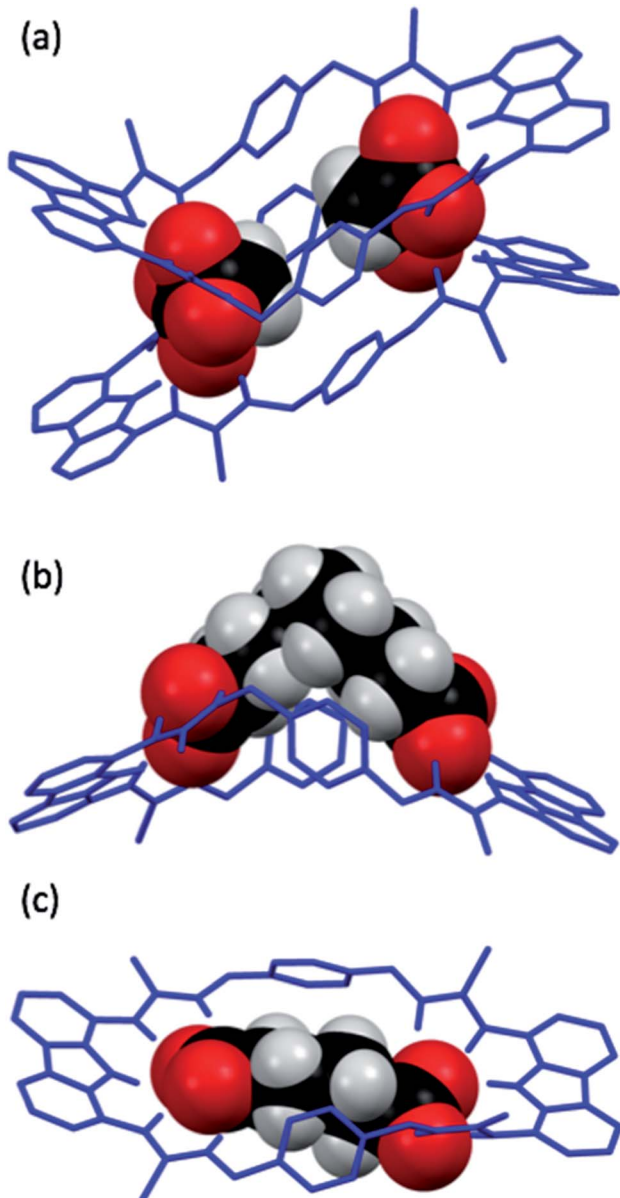


Fig. 7 X-ray crystal structures of **dt2** with various dicarboxylate guests, dicarboxylates are shown in spacefill mode with macrocycles as wire structures. In all cases, the TBA^+ cations, tertiary butyl groups on **dt2** and hydrogens not involved in intermolecular interactions on **dt2** have been removed for clarity. (a) **dt2·Mal**. (b) **dt2·Aze**. There are two macrocycles in this unit cell, both bound to **Aze** in a similar fashion, only one macrocycle is shown for clarity. (c) **dt2·Adi**.

In the solid state, the complex of **dt2** with **Mal** formed a [2+2] crystal structure (Fig. 7a), where each end of the dicarboxylate is bound to two different macrocycle molecules. A second dicarboxylate is bound to the other end of each macrocycle forming a cage. All eight thiocarbonyls on the macrocycles are pointing away from each other, along with the planar carbazole units. The xylol aromatic rings on both macrocycles are arranged in a staggered, planar conformation, however, centroid–centroid distances of 4.993 \AA and 4.819 \AA suggest no π – π interactions are occurring between neighbouring macrocycles. This indicates

that the cage is entirely held together by hydrogen bonding interactions from the macrocycles to the two dicarboxylate bridging units. It is clear that the **Mal** anion in this case is not large enough to span the distance between the two binding sites of an individual macrocycle. In this [2+2] complex, the two macrocycles in the structure are bent about their methylene units to accommodate both anions, the closest contact point between neighbouring macrocycles is from one thiourea NH to a second thiourea NH. This structure confirms the conclusions from the DMC analysis, indicating that oligomer formation is preferred in solution due to the anion being unable to span the two binding units of a single macrocycle.

The structure formed with **dt2·Aze** is quite different (Fig. 7b). Here, a 1 : 1 complex was formed where the anion, which is much larger than the macrocyclic pore, contorts from its favourable conformation in order to bind to both ends of the macrocycle. The macrocycle is also significantly twisted with all thiocarbonyls pointing down and away from each other. The anion is forced to adopt an unfavourable conformation, as supported by the DMC analysis, to allow it to bind to the receptor in a 1 : 1 manner. This conformational rearrangement from the preferred all-gauche conformer would be energetically unfavourable in solution. In addition, as the alkyl spacer on **Aze** is not encapsulated within the macrocycle pore, additional destabilisation may occur due to interactions between the non-polar alkyl chain and the polar solvent.

Contrastingly, the crystal structure of **dt2·Adi** shows the anion is almost perfectly encapsulated by the macrocycle and the overall complex is relatively planar (Fig. 7c), with a slight twist in the macrocycle to better encapsulate the entirety of the anion. Table 2 shows the measured macrocycle pore sizes ($\text{N}3\cdots\text{N}8$) for the three complexes **dt2·Mal**, **dt2·Adi** and **dt2·Aze**. In the structure for **dt2·Aze**, there are two macrocycle complexes in the unit cell, both showing similar geometry, only one complex is shown in Fig. 7b but both measured pore sizes are provided.

Interestingly, analysis of the macrocycle pore sizes shows that the complex with **Adi** has the largest $\text{N}\cdots\text{N}$ distance of the three crystals collected: 12.856 \AA for **dt2·Adi** versus 12.285 \AA for **dt2·Aze** (largest size) and 12.125 \AA for **dt2·Mal** (largest size). This confirms the semi-flexibility of macrocycle and shows that the pore size and therefore binding pocket is malleable. In this case, the planarization of the macrocycle gives an increased pore size of $\sim 0.6\text{ \AA}$ to better adapt to the added guest. The complimentary geometric matchup between **Adi** and **dt2** is

Table 2 Macrocyclic pore sizes for **dt2** measured from X-ray crystal structures various anions

	Macrocyclic number ^a	Pore size ^b (\AA)
dt2·Mal	1	12.077
	2	12.125
dt2·Adi	1	12.856
dt2·Aze	1	12.285
	2	11.435

^a Macrocyclic number in unit cell. ^b Pore size calculated by measuring the carbazole $\text{N}\cdots\text{N}$ distances ($\text{N}3\cdots\text{N}8$).



reflected in the high binding constant from titration studies and high positive cooperativity in DMC analysis. As a conformational change occurs upon binding, this is a clear indication of favourable energetics induced by increased cooperative effect towards forming the closed cyclic species.

Conclusions

To conclude, we have examined the anion binding of two differentially shaped ditopic macrocyclic receptors towards ditopic anionic guests in a competitive polar solvent. While surprisingly few discrepancies were observed between the binding affinities of the two hosts with flexible (unsaturated) guests, with rigid guests, larger differences in binding affinities between were observed due to geometric matches or mismatches. DMC analysis allowed the chelate cooperativity effects of these systems to be investigated. Negative cooperativity was observed in cases where the guest was too short to span the macrocycle pore. Negative cooperativity was also observed where the guest was much larger than the host pore, even though the guest can flex to bind both parts of the ditopic host as evidenced in the solid state; this is energetically unfavourable in solution. One reason for this may be due to a lack of favourable spacer interactions that occur when the host and guest fits are complimentary, which cannot occur if encapsulation of the guest is incomplete by the host. Conversely, positive cooperativity was observed where a flexible guest can span the length of the host and fit entirely within the macrocyclic pore. This cooperativity increases up to the optimal guest size and is rewarded with high EMs and binding constants and high selectivity over monotopic host/guest systems (selectivity for **dt2** for **adi** over **mt3** for **pro** is >175 times). Beyond the optimal guest size, the cooperative effect drops off rapidly. NMR and crystallographic studies have shown that the semi-flexible hosts can alter their pore size to better encapsulate guests and cooperativity analysis suggests that it is energetically favourable to do so. This work serves to further elucidate the subtle complexities between binding affinity and chelate cooperativity. While the ditopic binding of **Aze** was shown to be unfavourable, the binding constant is still an order of magnitude higher than the monotopic binding to the reference **Pro**. Furthermore, it serves to highlight how significant spacer interactions can stabilise or destabilise cooperative interactions, which will aid in future design for specific and selective supramolecular systems for multitopic receptors.

Conflicts of interest

There are no conflicts to declare.

Acknowledgements

This work was supported by the Australian Research Council (DP170100118 to K. A. J.). L. Q. thanks the University of Sydney for a Lambertson Scholarship. This work was facilitated by access to Sydney Analytical, a core research facility at The University of Sydney.

References

- B. Cornils and P. Lappe, in *Ullmann's Encyclopedia of Industrial Chemistry*, 2014, pp. 1–18.
- D. Curiel, M. Más-Montoya and G. Sánchez, *Coord. Chem. Rev.*, 2015, **284**, 19–66.
- A. M. Pajor, *J. Membr. Biol.*, 2000, **175**, 1–8.
- K. S. Oyedotun and B. D. Lemire, *J. Biol. Chem.*, 2004, **279**, 9424–9431.
- W. He, F. J. P. Miao, D. C. H. Lin, R. T. Schwandner, Z. Wang, J. Gao, J. L. Chen, H. Tlan and L. Ling, *Nature*, 2004, **429**, 188–193.
- I. Bechthold, K. Bretz, S. Kabasci, R. Kopitzky and A. Springer, *Chem. Eng. Technol.*, 2008, **31**, 647–654.
- N. Werner and S. Zibek, *World J. Microbiol. Biotechnol.*, 2017, **33**, 1–9.
- J. Ruprecht, V. Yankovskaya, E. Maklashina, S. Iwata and G. Cecchini, *J. Biol. Chem.*, 2009, **284**, 29836–29846.
- V. Yankovskaya, R. Horsefield, S. Tornroth, C. Luna-Chavez, H. Miyoshi, C. Leger, B. Byrne, G. Cecchini and S. Iwata, *Science*, 2003, **299**, 700–704.
- L. Valls-Lacalle, I. Barba, E. Miró-Casas, J. J. Alburquerque-Béjar, M. Ruiz-Meana, M. Fuertes-Agudo, A. Rodríguez-Sinovas and D. García-Dorado, *Cardiovasc. Res.*, 2016, **109**, 374–384.
- M. Más-Montoya, D. Curiel, C. Ramírez de Arellano, A. Tárraga and P. Molina, *Eur. J. Org. Chem.*, 2016, **2016**, 3878–3883.
- V. Korendovych, M. Cho, P. L. Butler, R. J. Staples and E. V. Rybak-Akimova, *Org. Lett.*, 2006, **8**, 3171–3174.
- T. Gunnlaugsson, A. P. Davis, J. E. O'Brien and M. Glynn, *Org. Biomol. Chem.*, 2005, **3**, 48–56.
- T. Gunnlaugsson, A. P. Davis, J. E. O'Brien and M. Glynn, *Org. Lett.*, 2002, **4**, 2449–2452.
- J. Y. C. Lim, I. Marques, V. Félix and P. D. Beer, *Angew. Chem., Int. Ed.*, 2018, **57**, 584–588.
- J. Y. C. Lim, I. Marques, V. Félix and P. D. Beer, *Chem. Commun.*, 2018, **54**, 10851–10854.
- A. D. Hughes and E. V. Anslyn, *Proc. Natl. Acad. Sci. U. S. A.*, 2007, **104**, 6538–6543.
- M.-P. Teulade-Fichou, J. Vigneron and J. Lehn, *J. Chem. Soc., Perkin Trans. 2*, 1996, **2**, 2169–2175.
- M. Hu and G. Feng, *Chem. Commun.*, 2012, **48**, 6951–6953.
- P. Mateus, R. Delgado, V. André and M. T. Duarte, *Inorg. Chem.*, 2015, **54**, 229–240.
- A. Ragusa, S. Rossi, J. M. Hayes, M. Stein and J. D. Kilburn, *Chem.-Eur. J.*, 2005, **11**, 5674–5688.
- S. Rossi, G. M. Kyne, D. L. Turner, N. J. Wells and J. D. Kilburn, *Angew. Chem., Int. Ed.*, 2002, **76**, 4233–4236.
- W. Chen, C. Guo, Q. He, X. Chi, V. M. Lynch, Z. Zhang, J. Su, H. Tian and J. L. Sessler, *J. Am. Chem. Soc.*, 2019, **141**, 14798–14806.
- Q. Q. Wang, V. W. Day and K. Bowman-James, *Chem. Sci.*, 2011, **2**, 1735–1738.
- C. Bravin, A. Guidetti, G. Licini and C. Zonta, *Chem. Sci.*, 2019, **10**, 3523–3528.



26 M. Pushina, P. Koutnik, R. Nishiyabu, T. Minami, P. Savechenkov and P. Anzenbacher, *Chem.-Eur. J.*, 2018, **24**, 4879–4884.

27 S. L. Wiskur, P. N. Floriano, E. V. Anslyn and J. T. McDevitt, *Angew. Chem., Int. Ed.*, 2003, **42**, 2070–2072.

28 G. Ercolani and L. Schiaffino, *Angew. Chem., Int. Ed.*, 2011, **50**, 1762–1768.

29 C. A. Hunter and H. L. Anderson, *Angew. Chem., Int. Ed.*, 2009, **48**, 7488–7499.

30 L. K. S. Von Krbek, C. A. Schalley and P. Thordarson, *Chem. Soc. Rev.*, 2017, **46**, 2622–2637.

31 A. Camara-Campos, D. Musumeci, C. A. Hunter and S. Turega, *J. Am. Chem. Soc.*, 2009, **131**, 18518–18524.

32 H. Adams, E. Chekmeneva, C. A. Hunter, M. C. Misuraca, C. Navarro and S. M. Turega, *J. Am. Chem. Soc.*, 2013, **135**, 1853–1863.

33 S. Henkel, M. C. Misuraca, Y. Ding, M. Guitet and C. A. Hunter, *J. Am. Chem. Soc.*, 2017, **139**, 6675–6681.

34 H. Sun, C. A. Hunter and E. M. Llamas, *Chem. Sci.*, 2015, **6**, 1444–1453.

35 L. K. S. von Krbek, A. J. Achazi, S. Schoder, M. Gaedke, T. Biberger, B. Paulus and C. A. Schalley, *Chem.-Eur. J.*, 2017, **23**, 2877–2883.

36 W. Jiang, K. Nowosinski, N. L. Löw, E. V. Dzyuba, F. Klautzsch, A. Schäfer, J. Huuskonen, K. Rissanen and C. A. Schalley, *J. Am. Chem. Soc.*, 2012, **134**, 1860–1868.

37 K. Nowosinski, L. K. S. Von Krbek, N. L. Traulsen and C. A. Schalley, *Org. Lett.*, 2015, **17**, 5076–5079.

38 C. Montoro-García, J. Camacho-García, A. M. López-Pérez, M. J. Mayoral, N. Bilbao and D. González-Rodríguez, *Angew. Chem., Int. Ed.*, 2016, **55**, 223–227.

39 G. Ercolani, *J. Am. Chem. Soc.*, 2003, **125**, 16097–16103.

40 M. C. Misuraca, T. Grecu, Z. Freixa, V. Garavini, C. A. Hunter, P. W. N. M. Van Leeuwen, M. D. Segarra-Maset and S. M. Turega, *J. Org. Chem.*, 2011, **76**, 2723–2732.

41 H. J. Hogben, J. K. Sprafke, M. Hoffmann, M. Pawlicki and H. L. Anderson, *J. Am. Chem. Soc.*, 2011, **133**, 20962–20969.

42 J. Raker and T. E. Glass, *J. Org. Chem.*, 2002, **67**, 6113–6116.

43 M. J. Chmielewski, M. Charon and J. Jurczak, *Org. Lett.*, 2004, **6**, 3501–3504.

44 M. Belén Jiménez, V. Alcázar, R. Peláez, F. Sanz, Á. L. Fuentes De Arriba and M. C. Caballero, *Org. Biomol. Chem.*, 2012, **10**, 1181–1185.

45 D. E. Gross, V. Mikkilineni, V. M. Lynch and J. L. Sessler, *Supramol. Chem.*, 2010, **22**, 135–141.

46 L. Qin, A. Hartley, P. Turner, R. B. P. Elmes and K. A. Jolliffe, *Chem. Sci.*, 2016, **7**, 4563–4572.

47 L. K. S. Von Krbek, A. J. Achazi, M. Solleeder, M. Weber, B. Paulus and C. A. Schalley, *Chem.-Eur. J.*, 2016, **27**, 15475–15484.

48 <http://www.supramolecular.org>, accessed March 2019.

